

Algorithms for Localization and Tracking of Acoustic Sources with Widely Separated Sensors

Richard J. Kozick
Bucknell University
Department of Electrical Engineering
Lewisburg, PA 17837

Brian M. Sadler
Army Research Laboratory
AMSRL CI CN
2800 Powder Mill Road
Adelphi, MD 20783

Abstract

Multiple sensor arrays distributed over a region provide the means for accurate localization of the (x, y) position of a source. When microphone arrays are used to measure aeroacoustic signals from ground vehicles, random fluctuations in the air lead to frequency-selective coherence of the signals that arrive at widely-separated arrays. We have shown previously that even in cases of imperfect spatial coherence, improvements in source localization accuracy are possible when the data from widely-separated arrays are processed jointly by a fusion center. Further, we have shown that a distributed processing scheme involving bearing estimation at individual arrays and time-delay estimation between pairs of widely-separated sensors performs nearly as well as the optimum scheme, with significantly lower communication bandwidth. These results were obtained by studying the Cramer-Rao bound (CRB) on source localization accuracy based on a statistical model for the data measured at the sensors. The contributions of this paper include the presentation of more accurate performance bounds (Ziv-Zakai), and the development of a narrowband subspace algorithm for source localization with distributed arrays and partially coherent signals. We demonstrate through analysis, simulation, and processing of measured data that the performance of both algorithms is limited by ambiguities that arise from the narrowband signals and the large spacing between arrays.

1 Introduction

We are concerned with estimating the location (x_s, y_s) of a wideband source using multiple sensor arrays that are distributed over an area. We consider schemes that distribute the processing between the individual arrays and a fusion center in order to limit the communication bandwidth between arrays and fusion center. Triangulation is a standard approach for source localization with multiple sensor arrays. Each array estimates a bearing and transmits the bearing to the fusion center, which combines the bearings to estimate the source location (x_s, y_s) . Triangulation is characterized by low communication bandwidth and low complexity, but it ignores *coherence* that may be present in the wavefronts that are received at distributed arrays. In this paper, we investigate new approaches for source localization with multiple arrays that exploit partial coherence of the wavefronts at distributed arrays. We have shown previously in [1] that the Cramer-Rao lower bound (CRB) on the variance of source location estimates is reduced when coherence from array to array is exploited. We also showed in [1] that the CRB changes little for suboptimum source localization methods that

Report Documentation Page

Report Date 23 Sep 2000	Report Type N/A	Dates Covered (from... to) -
Title and Subtitle Algorithms for Localization and Tracking of Acoustic Sources with Widely Separated Sensors		Contract Number
		Grant Number
		Program Element Number
Author(s)	Project Number	
	Task Number	
	Work Unit Number	
Performing Organization Name(s) and Address(es) Bucknell University Department of Electrical Engineering Lewisburg, PA 17837		Performing Organization Report Number
Sponsoring/Monitoring Agency Name(s) and Address(es) Department of the Army, CECOM RDEC Night Vision & Electronic Sensors Directorate AMSEL-RD-NV-D 10221 Burbeck Road Ft. Belvoir, VA 22060-5806		Sponsor/Monitor's Acronym(s)
		Sponsor/Monitor's Report Number(s)
Distribution/Availability Statement Approved for public release, distribution unlimited		
Supplementary Notes See also ADM201471, Papers from the Meeting of the MSS Specialty Group on Battlefield Acoustic and Seismic Sensing, Magnetic and Electric Field Sensors (2001) Held in Applied Physics Lab, Johns Hopkins Univ, Laurel, MD on 24-26 Oct 2001. Volume 2 (Also includes 1999 and 2000 Meetings), The original document contains color images.		
Abstract		
Subject Terms		
Report Classification unclassified	Classification of this page unclassified	
Classification of Abstract unclassified	Limitation of Abstract UU	
Number of Pages 19		

employ distributed processing to reduce the communication bandwidth between the arrays and the fusion center.

In this paper, we focus on the case of *narrowband* processing, and algorithms are investigated for source localization with partially coherent signals that are received by multiple distributed sensor arrays. Two algorithms are studied: one is based on estimating the time delay in the signals received by widely-separated arrays, and the other is a subspace algorithm. The algorithms are evaluated in terms of their ability to achieve the performance predicted by the CRBs developed in [1], and by processing data measured at Spesutie Island, Maryland. Our algorithms and testing address the issues of random propagation effects that result in partially coherent signals arriving at widely separated sensors, and Doppler effects due to source motion are compensated to improve the coherence.

The performance analysis presented in [1] is based on the Cramer-Rao lower bound (CRB) on the accuracy of any unbiased estimator of the source location. We model the signals measured at the distributed sensor arrays as jointly Gaussian wideband random processes. The model accounts for propagation effects between the source and the distributed arrays, including frequency-selective spatial coherence and different signal power spectra received at each array. The spatial coherence of the wavefronts is modeled as perfect over each individual array but imperfect between distinct arrays. This idealization allows us to study the effect of varying coherence between arrays on source localization accuracy. Physical modeling of frequency-selective coherence is discussed in [15]. The power spectral density of the source is arbitrary, allowing a range of cases to be modeled, including narrowband sources, sums of harmonics, and wideband sources with continuous power spectra.

Previous work on source localization with acoustical arrays has focused on angle of arrival estimation with a *single* array [2, 3, 4, 5]. These works use the coherent wideband focusing approach [6, 7] to combine correlation matrices from different narrowband frequency bins into a single correlation matrix that admits subspace processing. The problem of imperfect spatial coherence in the context of narrowband angle-of-arrival estimation with a single array has been studied in [8]-[11]. Pauraj and Kailath [8] presented a MUSIC algorithm that incorporates the nonideal spatial coherence, assuming that the coherence variation is known. Gershman et al. [9] provided a procedure to jointly estimate the spatial coherence loss and the angles of arrival. Song and Ritcey [10] provide maximum-likelihood methods for estimating the parameters of a coherence model and the angles of arrival, and Wilson [11] incorporates physical models for the spatial coherence. The problem of decentralized array processing has been studied in [12] and [13]. Wax and Kailath [12] present subspace algorithms for narrowband signals and distributed arrays, assuming perfect spatial coherence across each array but neglecting the spatial coherence between arrays. Weinstein [13] presents performance analysis for pairwise processing the wideband sensor signals from a single array and shows negligible loss in localization accuracy when the SNR is high.

The paper is organized as follows. Section 2 describes our model for partially coherent signals observed by the distributed sensor arrays. Also included in Section 2 are results from measured data to illustrate that partial signal coherence is present in measured aeroacoustic data with sensors separated by hundreds of meters. The CRB expressions for source location accuracy are reviewed in Section 3. Section 4 presents fundamental bounds on time-delay estimation that are an extension of the Ziv-Zakai bounds [14] to the case of partially coherent signals. Section 5 presents a novel subspace algorithm for narrowband source localization with distributed arrays and partially coherent signals. Examples of processing measured data are included in Sections 4 and 5, and Section 6 contains a brief discussion of our continuing work.

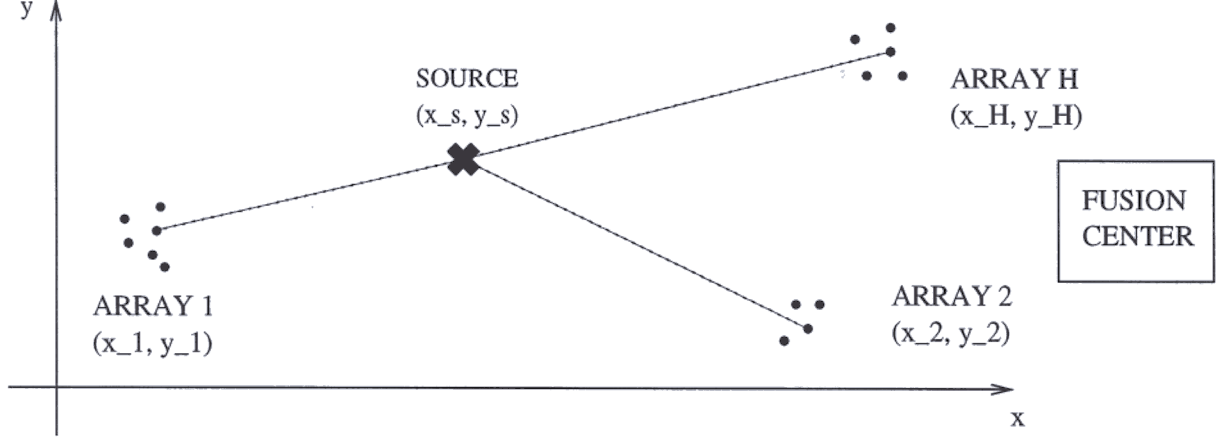


Figure 1: Geometry of source location and H distributed sensor arrays. A communication link is available between each array and the fusion center.

2 Data Model

A model is formulated in this section for the discrete-time signals received by the sensors in distributed arrays. Consider a single source that is located at coordinates (x_s, y_s) in the (x, y) plane. Then H arrays are distributed in the same plane, as illustrated in Figure 1. Each array $h \in \{1, \dots, H\}$ contains N_h sensors, and has a reference sensor located at coordinates (x_h, y_h) . The location of sensor $n \in \{1, \dots, N_h\}$ is at $(x_h + \Delta x_{hn}, y_h + \Delta y_{hn})$, where $(\Delta x_{hn}, \Delta y_{hn})$ is the relative location with respect to the reference sensor. If c is the speed of propagation, then the propagation time from the source to the reference sensor on array h is

$$\tau_h = \frac{r_h}{c} = \frac{1}{c} \left[(x_s - x_h)^2 + (y_s - y_h)^2 \right]^{1/2}. \quad (1)$$

We will assume that the wavefronts are well approximated by plane waves over the aperture of individual arrays. Then the propagation time from the source to sensor n on array h will be expressed by $\tau_h + \tau_{hn}$, where

$$\tau_{hn} \approx -\frac{1}{c} \left[\frac{x_s - x_h}{r_h} \Delta x_{hn} + \frac{y_s - y_h}{r_h} \Delta y_{hn} \right] = -\frac{1}{c} [(\cos \phi_h) \Delta x_{hn} + (\sin \phi_h) \Delta y_{hn}] \quad (2)$$

where τ_{hn} is the propagation time from the reference sensor on array h to sensor n on array h , and ϕ_h is the bearing of the source with respect to array h . Note that while the far-field approximation (2) is reasonable over individual array apertures, the wavefront curvature that is inherent in (1) must be retained in order to accurately model the (possibly) wide separation between arrays.

The time signal received at sensor n on array h due to the source will be represented as $s_h(t - \tau_h - \tau_{hn})$, where the vector of signals $\mathbf{s}(t) = [s_1(t), \dots, s_H(t)]^T$ received at the H arrays are modeled as real-valued, continuous-time, zero-mean, wide-sense stationary, Gaussian random processes with $-\infty < t < \infty$. These processes are fully specified by the $H \times H$ cross-correlation function matrix

$$\mathbf{R}_s(\tau) = E\{\mathbf{s}(t + \tau) \mathbf{s}(t)^T\}, \quad (3)$$

where E denotes expectation, superscript T denotes transpose, and we will later use the notation superscript $*$ and superscript H to denote complex conjugate and conjugate transpose, respectively. The (g, h) element in (3) is the cross-correlation function

$$r_{s,gh}(\tau) = E\{s_g(t + \tau) s_h(t)\} \quad (4)$$

between the signals received at arrays g and h . The correlation functions (3) and (4) are equivalently characterized by their Fourier transforms, which are the cross-spectral density functions

$$G_{s,gh}(\omega) = \mathcal{F}\{r_{s,gh}(\tau)\} = \int_{-\infty}^{\infty} r_{s,gh}(\tau) \exp(-j\omega\tau) d\tau \quad (5)$$

and the associated cross-spectral density matrix

$$\mathbf{G}_s(\omega) = \mathcal{F}\{\mathbf{R}_s(\tau)\}. \quad (6)$$

The diagonal elements $G_{s,hh}(\omega)$ of (6) are the power spectral density (PSD) functions of the signals $s_h(t)$, and hence they describe the distribution of average signal power with frequency. The model allows the average signal power to vary from one array to another. Indeed, the PSD may vary from one array to another to reflect propagation differences, source aspect angle differences, and other effects that lead to coherence degradation in the signals at distributed arrays.

Let us elaborate the definition and the meaning of *coherence* between the signals $s_g(t)$ and $s_h(t)$ received at distinct arrays g and h . In general, the cross-spectral density function (5) can be expressed in the form

$$G_{s,gh}(\omega) = \gamma_{s,gh}(\omega) [G_{s,gg}(\omega)G_{s,hh}(\omega)]^{1/2}, \quad (7)$$

where $\gamma_{s,gh}(\omega)$ is the spectral coherence function, which has the property $0 \leq |\gamma_{s,gh}(\omega)| \leq 1$. The coherence function $\gamma_{s,gh}(\omega)$ is generally complex-valued, but we will model it as real-valued. This is a reasonable assumption for acoustic propagation environments in which the loss of coherence is due to random changes in the propagation path length [11, 15]. Note that our assumption of perfect spatial coherence across individual arrays implies that the random changes in the propagation path length have negligible impact on the intra-array delays in (2). Thus the apparent bearing ϕ_h to array h remains fixed, but the inter-array path delays are randomly perturbed from their deterministic values given by (1). These random effects are modeled by the signal coherence function, $\gamma_{s,gh}(\omega)$.

We model the signal received at sensor n on array h as a sum of the delayed source signal and noise,

$$z_{hn}(t) = s_h(t - \tau_h - \tau_{hn}) + w_{hn}(t), \quad (8)$$

where the noise signals $w_{hn}(t)$ are modeled as real-valued, continuous-time, zero-mean, wide-sense stationary, Gaussian random processes that are uncorrelated at distinct sensors. That is, the noise correlation properties are

$$E\{w_{gm}(t + \tau)w_{hn}(t)\} = r_w(\tau) \delta_{gh}\delta_{mn}, \quad (9)$$

where $r_w(\tau)$ is the noise autocorrelation function, and the noise power spectral density is $G_w(\omega) = \mathcal{F}\{r_w(\tau)\}$. We then collect the observations at each array h into $N_h \times 1$ vectors

$\mathbf{z}_h(t) = [z_{h1}(t), \dots, z_{hN_h}(t)]^T$ for $h = 1, \dots, H$, and we further collect the observations from the H arrays into a $(N_1 + \dots + N_H) \times 1$ vector

$$\mathbf{Z}(t) = \begin{bmatrix} \mathbf{z}_1(t) \\ \vdots \\ \mathbf{z}_H(t) \end{bmatrix}. \quad (10)$$

The elements of $\mathbf{Z}(t)$ in (10) are zero-mean, wide-sense stationary, Gaussian random processes. We can express the cross-spectral density matrix of $\mathbf{Z}(t)$ in a convenient form with the following definitions. The array manifold for array h at frequency ω is

$$\mathbf{a}_h(\omega) = \begin{bmatrix} \exp(-j\omega\tau_{h1}) \\ \vdots \\ \exp(-j\omega\tau_{hN_h}) \end{bmatrix} = \begin{bmatrix} \exp[j\frac{\omega}{c}((\cos \phi_h)\Delta x_{h1} + (\sin \phi_h)\Delta y_{h1})] \\ \vdots \\ \exp[j\frac{\omega}{c}((\cos \phi_h)\Delta x_{hN_h} + (\sin \phi_h)\Delta y_{hN_h})] \end{bmatrix}. \quad (11)$$

using τ_{hn} from (2) and assuming that the sensors have omnidirectional response to sources in the plane of interest. Let us define the relative time delay of the signal at arrays g and h as

$$D_{gh} = \tau_g - \tau_h, \quad (12)$$

where τ_h is defined in (1). Then the cross-spectral density matrix of $\mathbf{Z}(t)$ in (10) has the form

$$\mathbf{G}_Z(\omega) = \begin{bmatrix} \mathbf{a}_1(\omega)\mathbf{a}_1(\omega)^H G_{s,11}(\omega) & \dots & \mathbf{a}_1(\omega)\mathbf{a}_H(\omega)^H \exp(-j\omega D_{1H})G_{s,1H}(\omega) \\ \vdots & \ddots & \vdots \\ \mathbf{a}_H(\omega)\mathbf{a}_1(\omega)^H \exp(+j\omega D_{1H})G_{s,1H}(\omega)^* & \dots & \mathbf{a}_H(\omega)\mathbf{a}_H(\omega)^H G_{s,HH}(\omega) \end{bmatrix} + G_w(\omega)\mathbf{I} \quad (13)$$

Recall that the source cross-spectral density functions $G_{s,gh}(\omega)$ in (13) can be expressed in terms of the spectral coherence $\gamma_{s,gh}(\omega)$ using (7).

Note that (13) depends on the source location parameters (x_s, y_s) through $\mathbf{a}_h(\omega)$ and D_{gh} . However, (13) points out that the observations are also characterized by the bearings ϕ_1, \dots, ϕ_H to the source from the individual arrays and the relative time delays D_{gh} between pairs of arrays. Therefore, one way to estimate the source location (x_s, y_s) is to estimate the bearings ϕ_1, \dots, ϕ_H and the pairwise time delays D_{gh} .

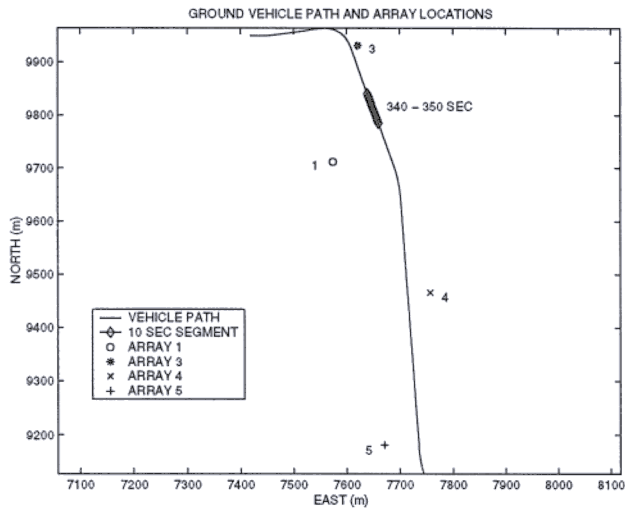
2.1 Signal coherence in measured data

Next we present results from measured aeroacoustic data to illustrate typical values of signal coherence at distributed arrays. The experimental setup is illustrated in Figure 2a, which shows the path of a moving ground vehicle and the locations of four microphone arrays (labeled 1, 3, 4, 5). Each array is circular with $N = 7$ sensors, 4-ft radius, and six sensors equally spaced around the perimeter with one sensor in the center. We focus on the 10 second segment indicated by the \diamond 's in Figure 2a (which correspond to the time segment 340-350 sec in the data). Figure 2b shows the power spectral density (PSD) of the data measured at arrays 1 and 3 during the 10 second segment. Note the dominant harmonic at 39 Hz. Figure 2c shows the estimated coherence between arrays 1 and 3 during the 10 second segment. The coherence is approximately 0.85 at 40 Hz, which demonstrates the presence of significant coherence at widely-separated microphones. Exploiting this coherence has the potential for improved source localization accuracy. Figure 2c shows the estimated coherence between two sensors on array 1, spaced by 8 feet. Note that the coherence is close to unity for frequencies in the range from about 40 to 200 Hz, so our model of perfect signal coherence over individual arrays seems reasonable.

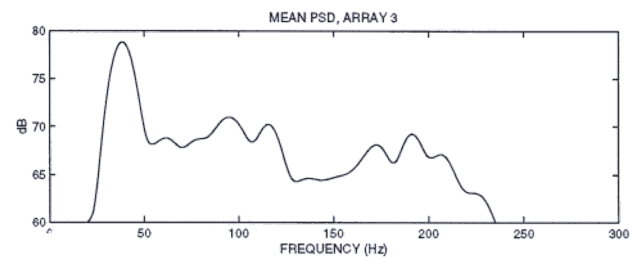
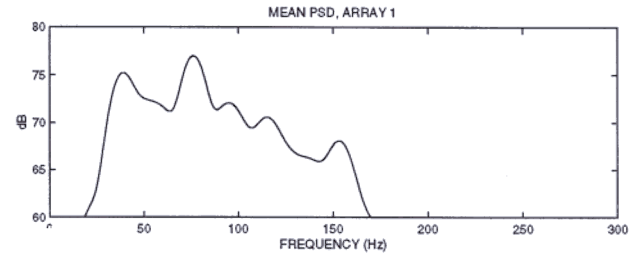
The Doppler effect due to source motion was compensated prior to the coherence estimate shown in Figure 2c. Without Doppler compensation, the coherence is significantly reduced, as shown in Figure 3a. The time-varying radial velocity of the source with respect to each array in Figure 2a is plotted in the top panel of Figure 3b. If $s(t)$ is the waveform emitted by the source that is moving with radial velocity v with respect to the sensor, then the sensor receives a waveform with the form $s(\alpha t)$, where the scaling factor α is

$$\alpha = 1 - \frac{v}{c} \quad (14)$$

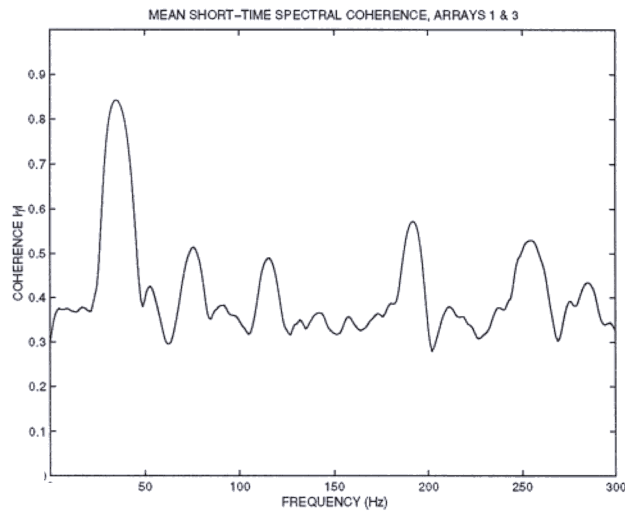
and c is the speed of wave propagation. The scaling factor α is plotted in the bottom panel of Figure 3b. Note that for this data set, $0.98 < \alpha < 1.02$, which corresponds to a Doppler frequency shift of approximately ± 1 Hz for an emitted tone at 50 hertz. We use a digital resampling algorithm to compensate for the Doppler effect.



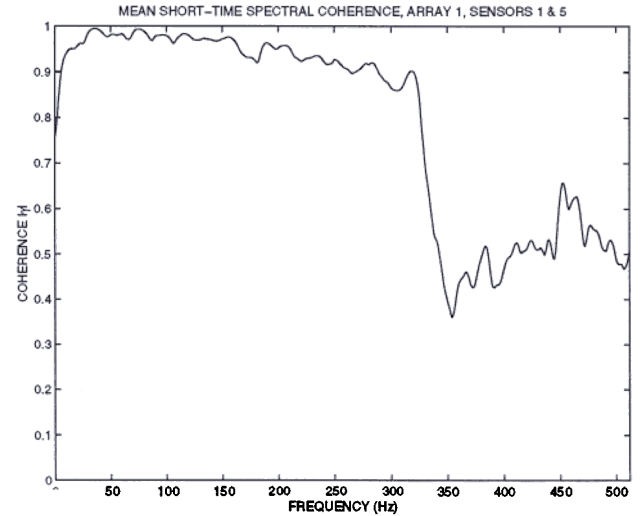
(a)



(b)



(c)



(d)

Figure 2: (a) Path of ground vehicle and array locations for measured data. (b) Mean power spectral density (PSD) at arrays 1 and 3 estimated from measured data over the 10 second segment \diamond in (b). Top panel is $G_{s,11}(f)$, bottom panel is $G_{s,33}(f)$. (c) Mean spectral coherence $\gamma_{s,13}(f)$ between arrays 1 and 3 estimated over the 10 second segment. (d) Mean spectral coherence for two sensors on array 1, with sensor spacing 8 feet.

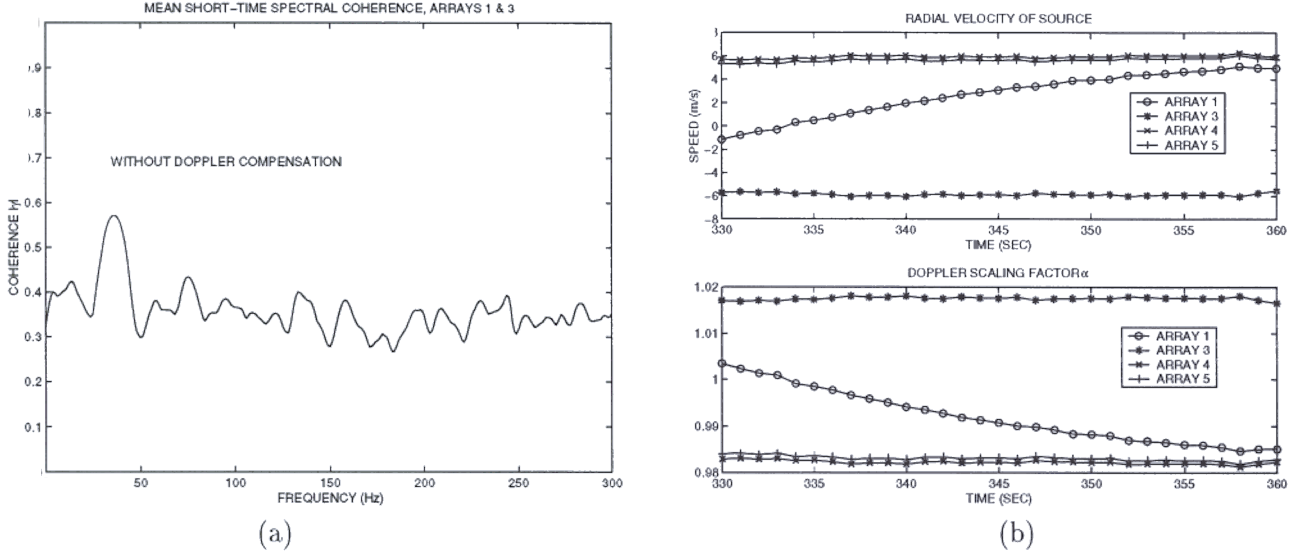


Figure 3: (a) Mean short-time spectral coherence between arrays 1 and 3 if Doppler is *not* compensated. (b) Radial velocity and Doppler scaling factor α in (14) for source in Figure 2a with respect to each array.

3 CRBs on Localization Accuracy

The problem of interest is to estimate the source location parameter vector $\Theta = [x_s, y_s]^T$ using T samples of the sensor signals $\mathbf{Z}(0), \mathbf{Z}(T_s), \dots, \mathbf{Z}((T-1) \cdot T_s)$, where T_s is the sampling period. Let us denote the sampling rate by $f_s = 1/T_s$ and $\omega_s = 2\pi f_s$. We will assume that the continuous-time random processes $\mathbf{Z}(t)$ are band-limited, and that the sampling rate f_s is greater than twice the bandwidth of the processes. Then Friedlander [18] has shown, using a theorem of Whittle [19], that the Fisher information matrix (FIM) \mathbf{J} for the parameters Θ based on the samples $\mathbf{Z}(0), \mathbf{Z}(T_s), \dots, \mathbf{Z}((T-1) \cdot T_s)$ has elements

$$J_{ij} = \frac{T}{2\omega_s} \int_0^{\omega_s} \text{tr} \left\{ \frac{\partial \mathbf{G}_Z(\omega)}{\partial \theta_i} \mathbf{G}_Z(\omega)^{-1} \frac{\partial \mathbf{G}_Z(\omega)}{\partial \theta_j} \mathbf{G}_Z(\omega)^{-1} \right\} d\omega, \quad i, j = 1, 2, \quad (15)$$

where “tr” denotes the trace of the matrix. The CRB matrix $\mathbf{C} = \mathbf{J}^{-1}$ then has the property that the covariance matrix of any unbiased estimator $\hat{\Theta}$ satisfies $\text{Cov}(\hat{\Theta}) - \mathbf{C} \geq \mathbf{0}$, where $\geq \mathbf{0}$ means that $\text{Cov}(\hat{\Theta}) - \mathbf{C}$ is positive semidefinite [17]. The CRB provides a lower bound on the performance of any unbiased estimator. Equation (15) provides a convenient way to compute the FIM for the distributed sensor array model. It provides a powerful tool for evaluating the impact that various parameters have on source localization accuracy. Parameters of interest include the spectral coherence between distributed arrays, the signal bandwidth and power spectrum, the array placement geometry, and the SNR. The FIM in (15) is not easily evaluated analytically, but it is readily evaluated numerically for cases of interest.

Consider an acoustic source that has a *narrowband* power spectrum. That is, the PSD $G_{s,hh}(\omega)$ of the signal at each array $h = 1, \dots, H$ is nonzero only in a narrow band of frequencies $\omega_0 -$

$(\Delta\omega/2) \leq \omega \leq \omega_0 + (\Delta\omega/2)$. If the bandwidth $\Delta\omega$ is chosen small enough so that the ω -dependent quantities in (15) are well approximated by their value at ω_0 , then the narrowband approximation to the FIM (15) is

$$J_{ij} \approx \frac{T\Delta\omega}{\omega_s} \text{tr} \left\{ \frac{\partial \mathbf{G}_Z(\omega_0)}{\partial \theta_i} \mathbf{G}_Z(\omega_0)^{-1} \frac{\partial \mathbf{G}_Z(\omega_0)}{\partial \theta_j} \mathbf{G}_Z(\omega_0)^{-1} \right\}.$$

The quantity $\frac{T\Delta\omega}{\omega_s}$ multiplying the FIM in (16) is the time-bandwidth product of the observations. In narrowband array processing, the T time samples per sensor are often segmented into M blocks containing T/M sample each. Then the discrete Fourier transform (DFT) is applied to each block, and the complex coefficients at frequency ω_0 (at each sensor) are used to form M array “snapshots”. In this case, the quantity $\frac{T\Delta\omega}{\omega_s}$ is approximately equal to M .

4 Threshold Coherence for Time Delay Estimation

In this section, we present a model for partial signal coherence in terms of an equivalent additive noise component, which allows the fundamental bounds on time delay estimation in [14] to be extended to the case of partially coherent signals. Bounds on time delay estimation are important because one of the suboptimum processing methods proposed in [1] for distributed processing with low communication bandwidth requires time delay estimation between widely separated sensors. The fundamental bounds in [14] are useful because they specify the required signal-to-noise ratio (SNR) such that the CRB is attainable. That is, if the SNR is less than a threshold, then the CRB on source localization accuracy is an optimistic and unattainable lower bound. We will show that for signals that are partially coherent when received at the sensors, a threshold phenomenon occurs with respect to *coherence*. That is, the signal coherence must exceed a threshold in order for the CRBs to be attainable. The existence of a threshold phenomenon for signal coherence is a useful refinement of [1], since the CRBs in [1] are formulated without regard for the conditions of attainability.

The appendix presents a decomposition of partially coherent signals into a coherent component and an incoherent additive noise component. Consider estimation of the time delay D in the model presented as (54),(55) and (64),(65) in the appendix. Let us specialize to narrowband processing, with signal bandwidth $\Delta\omega$ centered at ω_0 and observation time T seconds. Further, we assume that the signal power is identical at each sensor, and we define the following constants for notational simplicity:

$$G_{s,11}(\omega_0) = G_{s,2}(\omega_0) = G_s, \quad G_w(\omega_0) = G_w, \quad \gamma_{s,12}(\omega_0) = \gamma_s. \quad (17)$$

Then combining the formulation in the appendix with the development in [14], we can show that the following SNR expression characterizes the performance of time delay estimation with partially coherent signals:

$$\text{SNR}(\gamma_s) = \frac{|\gamma_s|^2 \left(\frac{G_s}{G_w} \right)^2}{\left[1 + (1 - |\gamma_s|) \left(\frac{G_s}{G_w} \right) \right]^2 + 2|\gamma_s| \left(\frac{G_s}{G_w} \right) \left[1 + (1 - |\gamma_s|) \left(\frac{G_s}{G_w} \right) \right]}. \quad (18)$$

From [14], the threshold SNR for CRB attainability in the narrowband time delay estimation problem is

$$\text{SNR}_{\text{thresh}} = \frac{6}{\pi^2 \left(\frac{\Delta\omega T}{2\pi} \right)} \left(\frac{\omega_0}{\Delta\omega} \right)^2 \left[\phi^{-1} \left(\frac{(\Delta\omega)^2}{24\omega_0^2} \right) \right]^2 \quad (19)$$

where $\phi(y) = 1/\sqrt{2\pi} \int_y^\infty \exp(-t^2/2) dt$. Thus

$$\text{SNR}(\gamma_s) \geq \text{SNR}_{\text{thresh}} \quad (20)$$

identifies the values of signal coherence γ_s and signal/noise PSDs G_s/G_w for CRB attainability. We can combine (18) with (20) to obtain the condition for CRB attainability

$$\frac{G_s}{G_w} \geq \frac{1}{|\gamma_s| \left(1 + \frac{1}{\text{SNR}_{\text{thresh}}}\right)^{1/2} - 1}, \quad (21)$$

which is possible only if

$$|\gamma_s|^2 \geq \frac{1}{1 + \frac{1}{\text{SNR}_{\text{thresh}}}}. \quad (22)$$

For a specific narrowband time delay estimation scenario, the threshold SNR for CRB attainability is given by (19), and (22) provides a corresponding threshold coherence for CRB attainability.

For example, consider time delay estimation in a band centered at $\omega_0 = 2\pi 50$ rad/sec using a time segment of duration 2 seconds.

- For a 1 Hz bandwidth, i.e., $\Delta\omega = 2\pi$ rad/sec, nearly *perfect* coherence ($\gamma_s = 0.99995$) is required in order to enter the regime of CRB attainability.

For a 10 Hz bandwidth, i.e. $\Delta\omega = 2\pi 10$ rad/sec, the coherence must exceed 0.93 for CRB attainability.

The implication is that for the narrowband signals with $\Delta\omega = 2\pi$ rad/sec, any loss of coherence leads to difficulty with time delay estimation due to ambiguities arising from the narrowband signals. But for sufficiently wideband signals, e.g., $\Delta\omega = 2\pi 10$ rad/sec, a certain amount of coherence loss can be tolerated while still allowing unambiguous time delay estimation.

We present an illustration based on processing the measured data for the source in Figure 2a. Figure 4 shows results of cross-correlation processing of the data for a 2 second segment at time 342 seconds. Figure 4a is obtained by cross-correlating the signals received at arrays 1 and 3, for which the coherence is appreciable only over a narrow band near 39 Hz. A peak in the cross-correlation is not evident, which is expected based on the preceding analysis, since nearly *perfect* coherence is needed for narrowband time delay estimation in this scenario. Figure 4b is obtained by cross-correlating the signals received at two sensors on array 1, where the coherence is as shown in Figure 2d. Due to the high signal coherence over a wide band, a peak is clearly evident in the cross-correlation.

5 Subspace Processing

In this section, we begin with an eigenanalysis of the cross-spectral density matrix (13) for the case of $H = 2$ arrays containing $N_1 = N_2 = N$ sensors operating in a narrow band of frequencies centered at ω_0 . This analysis leads to a MUSIC-like subspace algorithm for source localization with distributed arrays and partial signal coherence. We illustrate with computer simulations and measured aeroacoustic data that the new subspace algorithm is limited in performance due to source location ambiguities that arise from the large separation between arrays and the narrowband signals.

To simplify notation, we will let \mathbf{a}_h represent the array manifold $\mathbf{a}_h(\omega_0)$, σ_h^2 represent the average signal power at array h in the frequency band of interest, σ_w^2 is the average noise power, and γ is

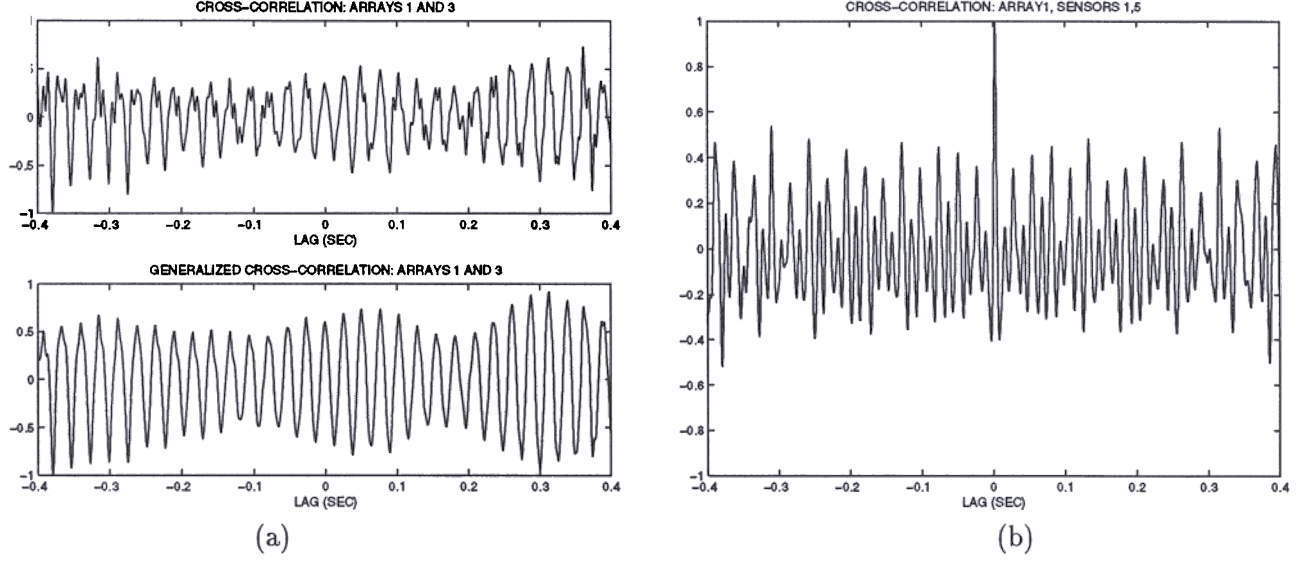


Figure 4: (a) Cross-correlation of signals at arrays 1 and 3 in Figure 2a for source at time 342 sec
(b) Cross-correlation of signals at two sensors on array 1, separated by 8 feet.

the coherence $\gamma_{s,12}(\omega_0)$. We allow γ to be complex-valued with $|\gamma| \leq 1$. Then (13) can be expressed as the correlation matrix

$$\mathbf{R}^{(12)} = \left(\begin{bmatrix} \sigma_1^2 & \gamma \sigma_1 \sigma_2 \\ \gamma^* \sigma_1 \sigma_2 & \sigma_2^2 \end{bmatrix} \otimes \mathbf{1}_{N \times N} \right) \circ \begin{bmatrix} \mathbf{a}_1 \mathbf{a}_1^H & \mathbf{a}_1 \mathbf{a}_2^H \exp(-j\omega_0 D_{12}) \\ \mathbf{a}_2 \mathbf{a}_1^H \exp(+j\omega_0 D_{12}) & \mathbf{a}_2 \mathbf{a}_2^H \end{bmatrix} + \sigma_w^2 \mathbf{I}, \quad (23)$$

where \otimes denotes Kronecker product, \circ denotes elementwise product, and $\mathbf{1}_{N \times N}$ is an $N \times N$ matrix of 1's. The superscript (12) in (23) indicates that the quantity is the combined correlation matrix of all sensors in arrays 1 and 2. The correlation matrices for the individual arrays 1 and 2 are

$$\mathbf{R}^{(h)} = \sigma_h^2 \mathbf{a}_h \mathbf{a}_h^H + \sigma_w^2 \mathbf{I}, \quad h = 1, 2. \quad (24)$$

It is well-known that the individual array correlation matrices $\mathbf{R}^{(1)}$ and $\mathbf{R}^{(2)}$ in (24) have a rank-1 signal subspace, and that the signal subspace eigenvalue is

$$\lambda_1^{(h)} = N\sigma_h^2 + \sigma_w^2, \quad h = 1, 2 \quad (25)$$

with corresponding eigenvector

$$\mathbf{e}_1^{(h)} = \mathbf{a}_h, \quad h = 1, 2. \quad (26)$$

The remaining eigenvalues $\lambda_n^{(h)}$, $n = 2, \dots, N$ are equal to σ_w^2 .

Now we present the eigenanalysis of the combined correlation matrix $\mathbf{R}^{(12)}$ in (23). The derivation of these results is similar to the reasoning in the appendix of [8]. We assume that the arrays are labeled so that $\sigma_1^2 \geq \sigma_2^2$, and that the sensors are omnidirectional so that the array manifold

elements are of the form $[a_h]_n = \exp(-j\omega_0 \tau_{hn})$. The rank of the signal subspace component of $R^{(12)}$ is at most two, and the two largest eigenvalues are

$$\lambda_1^{(12)} = \frac{N}{2} (\sigma_1^2 + \sigma_2^2) \left[1 + \sqrt{1 - (1 - |\gamma|^2) \left(\frac{2}{\frac{\sigma_1}{\sigma_2} + \frac{\sigma_2}{\sigma_1}} \right)^2} \right] + \sigma_w^2 \quad (27)$$

$$\lambda_2^{(12)} = \frac{N}{2} (\sigma_1^2 + \sigma_2^2) \left[1 - \sqrt{1 - (1 - |\gamma|^2) \left(\frac{2}{\frac{\sigma_1}{\sigma_2} + \frac{\sigma_2}{\sigma_1}} \right)^2} \right] + \sigma_w^2. \quad (28)$$

The corresponding eigenvectors are

$$\mathbf{e}_1^{(12)} = \begin{bmatrix} \frac{1}{2} \left(\frac{\sigma_1}{\sigma_2} - \frac{\sigma_2}{\sigma_1} \right) \left[1 + \sqrt{1 + \left(\frac{2|\gamma|}{\frac{\sigma_1}{\sigma_2} - \frac{\sigma_2}{\sigma_1}} \right)^2} \right] \mathbf{a}_1 \\ \gamma^* \exp(j\omega_0 D_{12}) \mathbf{a}_2 \end{bmatrix} \quad (29)$$

$$\mathbf{e}_2^{(12)} = \begin{bmatrix} -\gamma \mathbf{a}_1 \\ \frac{1}{2} \left(\frac{\sigma_1}{\sigma_2} - \frac{\sigma_2}{\sigma_1} \right) \left[1 + \sqrt{1 + \left(\frac{2|\gamma|}{\frac{\sigma_1}{\sigma_2} - \frac{\sigma_2}{\sigma_1}} \right)^2} \right] \exp(j\omega_0 D_{12}) \mathbf{a}_2 \end{bmatrix}, \quad (30)$$

provided $\sigma_1 \neq \sigma_2$. Some observations are as follows.

- In the case that $\sigma_1 = \sigma_2 = \sigma_s$, (27)-(30) reduce to

$$\lambda_1^{(12)} = N\sigma_s^2(1 + |\gamma|) + \sigma_w^2, \quad \lambda_2^{(12)} = N\sigma_s^2(1 - |\gamma|) + \sigma_w^2 \quad (31)$$

$$\mathbf{e}_1^{(12)} = \begin{bmatrix} \mathbf{a}_1 \\ (\gamma^*/|\gamma|) \exp(j\omega_0 D_{12}) \mathbf{a}_2 \end{bmatrix}, \quad \mathbf{e}_2^{(12)} = \begin{bmatrix} -(\gamma/|\gamma|) \mathbf{a}_1 \\ \exp(j\omega_0 D_{12}) \mathbf{a}_2 \end{bmatrix}. \quad (32)$$

Note that (32) is valid as long as $\gamma \neq 0$, and in this case the eigenvectors are independent of the coherence magnitude. In the case of high SNR so that $\sigma_w^2 \ll N\sigma_s^2(1 - |\gamma|)$, the ratio of signal eigenvalues is approximately

$$\frac{\lambda_1^{(12)}}{\lambda_2^{(12)}} \approx 1 + 2 \frac{|\gamma|}{1 - |\gamma|}. \quad (33)$$

From (33), in order for $\lambda_1^{(12)} > 10\lambda_2^{(12)}$ so that $\lambda_1^{(12)}$ is the dominant eigenvalue, the coherence must satisfy $|\gamma| > 0.8181$.

- In the case of perfect coherence $|\gamma| = 1$, $R^{(12)}$ has a rank-1 signal subspace, with signal eigenvalue and eigenvector

$$\lambda_1^{(12, COH)} = N(\sigma_1^2 + \sigma_2^2) + \sigma_w^2, \quad \mathbf{e}_1^{(12, COH)} = \begin{bmatrix} \sigma_1 \mathbf{a}_1 \\ \sigma_2 \gamma^* \exp(j\omega_0 D_{12}) \mathbf{a}_2 \end{bmatrix}. \quad (34)$$

The expressions in (34) are the natural extension of (25) and (26) applied to the “superarray” of all sensors, allowing for different signal power levels at the two arrays.

- In the case of partial coherence $|\gamma| < 1$, $R^{(12)}$ has a rank-2 signal subspace. The signal eigenvalues are ordered $\lambda_1^{(12)} \geq \lambda_2^{(12)}$, with equality if and only if $\gamma = 0$ and $\sigma_1 = \sigma_2$. In the incoherent case $\gamma = 0$, the signal eigenvectors are

$$\mathbf{e}_1^{(12, INC)} = \begin{bmatrix} \mathbf{a}_1 \\ 0 \end{bmatrix}, \quad \mathbf{e}_2^{(12, INC)} = \begin{bmatrix} 0 \\ \mathbf{a}_2 \end{bmatrix}. \quad (35)$$

Thus in the incoherent case, the signal eigenvectors (35) of $\mathbf{R}^{(12)}$ are completely determined by the signal eigenvectors (26) of individual array correlation matrices $\mathbf{R}^{(1)}$ and $\mathbf{R}^{(2)}$.

- Note that the span of the $\mathbf{R}^{(12)}$ signal subspace eigenvectors in (29) and (30) is *equal* to the span of the incoherent eigenvectors in (35). Therefore, for $|\gamma| < 1$, the signal subspace of $\mathbf{R}^{(12)}$ is spanned by the signal subspace eigenvectors of the *individual* array correlation matrices $\mathbf{R}^{(1)}$ and $\mathbf{R}^{(2)}$. It follows that $\mathbf{R}^{(12)}$ and the block diagonal matrix $\begin{bmatrix} \mathbf{R}^{(1)} & \mathbf{0} \\ \mathbf{0} & \mathbf{R}^{(2)} \end{bmatrix}$ have identical signal and noise subspaces. Thus a subspace algorithm that exploits *joint* processing of the two arrays must exploit the structure of the dominant signal subspace eigenvector $\mathbf{e}_1^{(12)}$ in (29).

The following subspace procedure may be used to estimate the source location (x_s, y_s) using the correlation matrices $\mathbf{R}^{(1)}$, $\mathbf{R}^{(2)}$, and $\mathbf{R}^{(12)}$.

1. Form the correlation matrices $\mathbf{R}^{(1)}$ and $\mathbf{R}^{(2)}$ using the observations from the individual arrays. Estimate the noise power σ_w^2 from the noise eigenvalues of $\mathbf{R}^{(1)}$ and $\mathbf{R}^{(2)}$. Then estimate the signal power at each array using the largest eigenvalue of $\mathbf{R}^{(1)}$ and $\mathbf{R}^{(2)}$ with (25):

$$\sigma_h^2 = \frac{1}{N} (\lambda_1^{(h)} - \sigma_w^2), \quad h = 1, 2. \quad (36)$$

2. Form the joint correlation matrix $\mathbf{R}^{(12)}$, and estimate the coherence magnitude $|\gamma|$ using the two largest eigenvalues $\lambda_1^{(12)}, \lambda_2^{(12)}$ of $\mathbf{R}^{(12)}$ with (27) and (28):

$$|\gamma| = \left[1 - \frac{1 - \left(\frac{\lambda_1^{(12)} - \lambda_2^{(12)}}{N(\sigma_1^2 + \sigma_2^2)} \right)^2}{\left(\frac{2}{\frac{\sigma_1}{\sigma_2} + \frac{\sigma_2}{\sigma_1}} \right)^2} \right]^{1/2}, \quad (37)$$

as long as $\sigma_1 \neq \sigma_2$. Note that if $\sigma_1 = \sigma_2$, then it is not necessary to estimate the coherence magnitude (see (32) and step 3 below). We will assume that γ is real-valued and positive, which is motivated by physical considerations as discussed earlier in this paper and in [11, 15].

3. Use the estimates for σ_1, σ_2 , and $|\gamma|$ in the signal eigenvector expression for $\mathbf{e}_1^{(12)}$ in (29) to create a “search vector” \mathbf{g} :

$$\mathbf{g}(x_s, y_s) = \begin{bmatrix} \frac{1}{2} \left(\frac{\sigma_1}{\sigma_2} - \frac{\sigma_2}{\sigma_1} \right) \left[1 + \sqrt{1 + \left(\frac{2|\gamma|}{\frac{\sigma_1}{\sigma_2} - \frac{\sigma_2}{\sigma_1}} \right)^2} \right] \mathbf{a}_1 \\ \gamma^* \exp(j\omega_0 D_{12}) \mathbf{a}_2 \end{bmatrix} = \begin{bmatrix} \beta_1 \mathbf{a}_1 \\ \gamma^* \exp(j\omega_0 D_{12}) \mathbf{a}_2 \end{bmatrix}, \quad (38)$$

where $\mathbf{a}_1, \mathbf{a}_2$, and D_{12} are functions of the source location (x_s, y_s) . (If $\sigma_1 = \sigma_2$, then the search vector is based on $\mathbf{e}_1^{(12)}$ in (32) instead.)

4. Let $\mathbf{e}_n^{(12)}$, $n = 1, \dots, 2N$ denote the eigenvectors of $\mathbf{R}^{(12)}$, ordered such that the corresponding eigenvalues follow $\lambda_1^{(12)} \geq \dots \geq \lambda_{2N}^{(12)}$. Then form the matrix

$$\mathbf{V} = \begin{bmatrix} \mathbf{e}_2^{(12)} & \dots & \mathbf{e}_{2N}^{(12)} \end{bmatrix}. \quad (39)$$

A MUSIC-type spectrum may then be defined as

$$P_c(x_s, y_s) = \frac{1}{\mathbf{g}^H \mathbf{V} \mathbf{V}^H \mathbf{g}}, \quad (40)$$

and the value of (x_s, y_s) that maximizes (40) is an estimate of the source location.

5. Wax and Kailath [12] proposed an “incoherent” MUSIC-type source location estimator that ignores coherence between the arrays. The form of the Wax and Kailath estimator can be expressed as follows,

$$P_i(x_s, y_s) = \frac{1}{\mathbf{a}_1^H \mathbf{V}^{(1)} \mathbf{V}^{(1)H} \mathbf{a}_1 + \mathbf{a}_2^H \mathbf{V}^{(2)} \mathbf{V}^{(2)H} \mathbf{a}_2} \quad (41)$$

where $\mathbf{V}^{(h)} = [\mathbf{e}_2^{(h)}, \dots, \mathbf{e}_N^{(h)}]$ contains the noise eigenvectors of $\mathbf{R}^{(h)}$

This analysis extends to the case of H arrays with a single source. If the signals are partially coherent at all arrays, then the dimension of the signal subspace of the combined correlation matrix is H . If K signals are present, then the combined correlation matrix has signal subspace with rank KH .

5.1 Examples of subspace processing

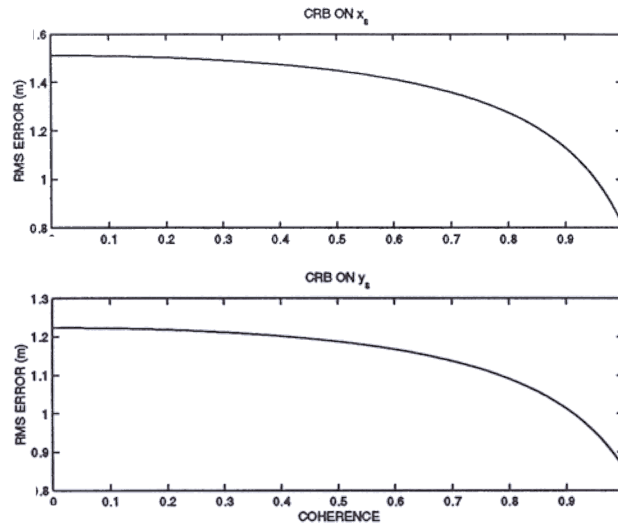
We present examples of the “partially coherent” MUSIC algorithm (40) and the “incoherent” MUSIC algorithm (41) with computer simulations and measured data. First, we simulate a scenario with $H = 2$ arrays. The individual arrays are identical and contain $N_1 = N_2 = N = 7$ sensors. Each array is circular and has 4-ft radius, with six sensors equally spaced around the perimeter and one sensor in the center. Narrowband processing centered at 40 Hz is assumed, with an SNR of 40 dB per sensor at array 1 and 34 dB at array 2, i.e., $G_{s,11}(\omega)/G_w(\omega) = 10^4$, $G_{s,22}(\omega)/G_w(\omega) = 2500$. The coherence is set to two values, $\gamma_{s,12} = 0.9$ and 0.999. The arrays are located at coordinates $(x_1, y_1) = (0, 150)$, $(x_2, y_2) = (0, 0)$, and one source is located at $(x_s, y_s) = (200, 300)$, where the units are meters. Source location estimation is performed using $M = 30$ snapshots, where each snapshot contains an estimate of the measured complex amplitude at 40 Hz at each sensor.

Results are presented in Figure 5, where part a shows an approximate CRB as a function of signal coherence.¹ Increasing coherence leads to modest improvement in the localization potential. Figures 5b and 5c contain representative spectra of incoherent and partially coherent MUSIC, respectively, for coherence $\gamma_{s,12} = 0.9$. Note that the incoherent MUSIC spectrum has a rather broad but unique maximum. The partially coherent MUSIC spectrum has a sharp ridge in one direction, with multiple peaks along the ridge. The multiple peaks arise due to the ambiguities in source location caused by the narrowband signals and large separation between arrays.

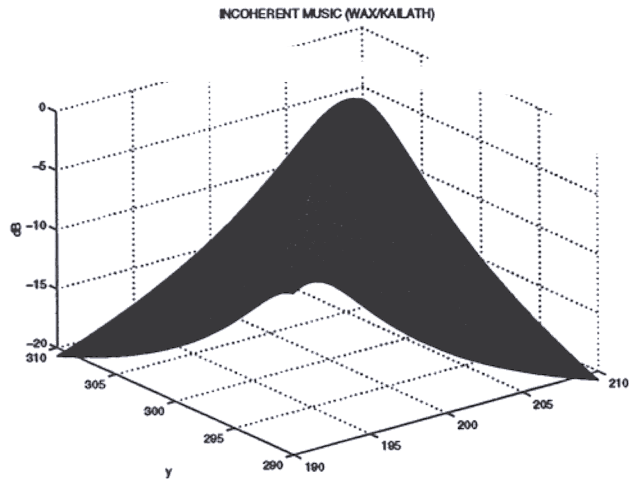
Table 1 contains results of Monte Carlo simulations with 100 runs for both coherence values, $\gamma_{s,12} = 0.9$ and 0.999. The incoherent MUSIC performs close to the approximate CRB in Figure 5a corresponding to $\gamma_{s,12} = 0$. Partially coherent MUSIC performs *worse* than incoherent MUSIC because of the ambiguities: partially coherent MUSIC sometimes chooses the incorrect peak along the ridge in the spectrum shown in Figure 5c. Note that partially coherent MUSIC is more accurate for $\gamma_s = 0.999$ than for $\gamma_s = 0.9$, suggesting that the ambiguities are less severe when the signal coherence is larger.

We have applied incoherent MUSIC and partially coherent MUSIC to the measured data scenario in Figure 2. The data is processed in a narrow band around 39 Hz for the 2-second interval between 345 and 347 seconds. Both algorithms produce identical estimates for the source location in this case, but the spectra for partially coherent MUSIC are shown in Figure 6. The top panel clearly shows the ambiguities that limit the performance with narrowband signals. The contour plot in the bottom panel also shows the periodic structure of the ambiguities.

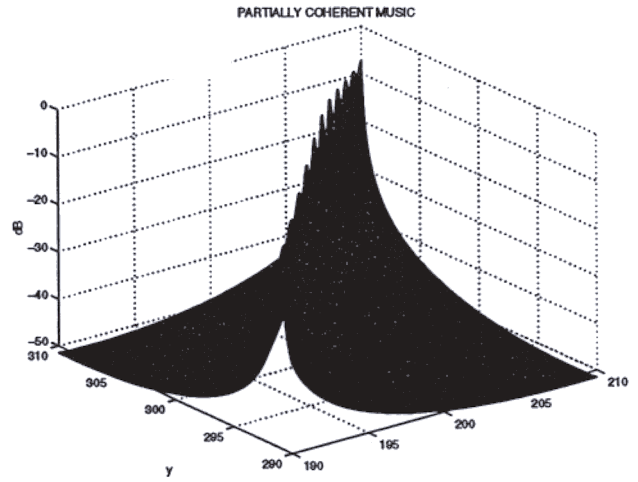
¹The CRB is approximate because the mapping of the scaling factor $\frac{T\Delta\omega}{\omega_s}$ in (16) to the number of snapshots M is approximate.



(a)



(b)



(c)

Figure 5: (a) CRBs on localization accuracy. (b) Incoherent MUSIC and (c) partially coherent MUSIC spectra.

Coherence	Approx. CRB		Incoherent MUSIC		Partially Coherent MUSIC	
	x_s	y_s	x_s	y_s	x_s	y_s
0.9	1.17	1.10	1.36	1.10	2.14	1.71
0.999	0.81	0.87	1.41	1.16	1.96	1.61
0.0	1.50	1.22				

Table 1: RMS error in simulation results for incoherent and partially coherent MUSIC.

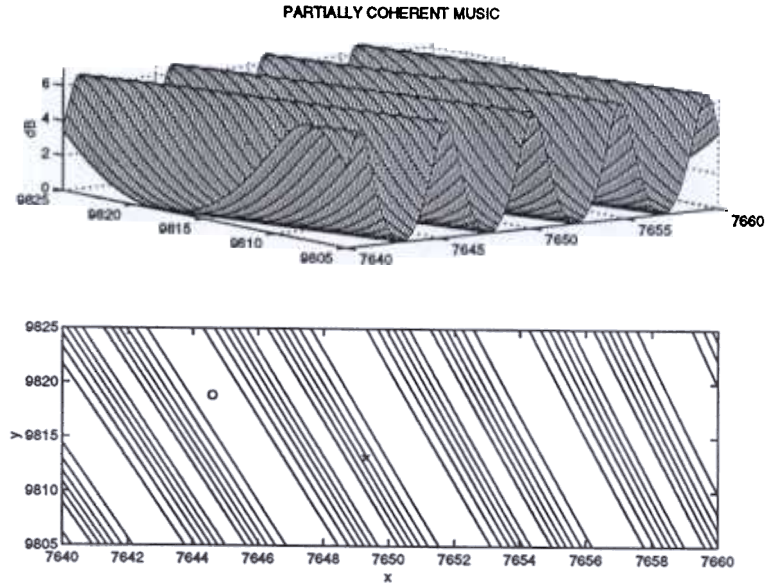


Figure 6: Partially coherent MUSIC spectrum for measured data.

6 Concluding Remarks

Items of continuing work include the following.

- The analysis in this paper was focused primarily on *narrowband* processing. We found that source location ambiguities due to the narrowband signals are an important limitation when distributed arrays are processed jointly. Signals that maintain coherence over a wider bandwidth are expected to experience fewer problems with ambiguities, so we are evaluating algorithms for this scenario.
- We are continuing to process measured data, particularly data from distributed arrays with synchronized sampling at the arrays, courtesy of Sanders Corporation.
- We are investigating models for the source motion that will improve accuracy and allow tracking.
- We are investigating extensions to the case of tracking multiple moving sources.

Appendix

A Equivalent Additive Noise Model for Coherence

The formulation in this appendix begins with Gaussian random variables for simplicity, and then the formulation is extended to Gaussian random processes.

Let X and Y be two complex, circular, Gaussian random variables with zero mean and

$$E\{|X|^2\} = \sigma_X^2, E\{|Y|^2\} = \sigma_Y^2, E\{XY^*\} = \rho\sigma_X\sigma_Y \quad (42)$$

Then X and Y can be expressed as

$$X = \sigma_X S + N_1 \quad (43)$$

$$Y = \frac{\rho^*}{|\rho|} \sigma_Y S + N_2, \quad (44)$$

where S, N_1, N_2 are independent, zero mean, complex, circular Gaussian random variables with

$$E\{|S|^2\} = |\rho| \quad (45)$$

$$E\{|N_1|^2\} = \sigma_X^2 (1 - |\rho|) \quad (46)$$

$$E\{|N_2|^2\} = \sigma_Y^2 (1 - |\rho|). \quad (47)$$

The relations in (42) can be verified using (43)-(47). Note that for X , the “coherent” part $\sigma_X S$ has variance $|\rho|\sigma_X^2$, while the “incoherent” part N_1 has variance $(1 - |\rho|)\sigma_X^2$. As $|\rho|$ decreases, a larger portion of σ_X^2 is applied to N_1 , so the incoherent noise gets stronger.

Suppose that X and Y described by (42) are observed in noise,

$$Z_1 = X + W_1 = \sigma_X S + N_1 + W_1 \quad (48)$$

$$Z_2 = Y + W_2 = \frac{\rho^*}{|\rho|} \sigma_Y S + N_2 + W_2, \quad (49)$$

where W_1 and W_2 are independent, zero mean, complex, circular Gaussian random variables with variance σ_W^2 , and W_1, W_2 are independent of X, Y (and therefore S, N_1, N_2). If we define the SNR of Z_1 and Z_2 based only on the *coherent* signal component, then

$$\text{SNR}_1 = \frac{|\rho| \sigma_X^2}{\sigma_W^2 + (1 - |\rho|) \sigma_X^2} = \frac{|\rho|}{\frac{\sigma_W^2}{\sigma_X^2} + (1 - |\rho|)} \quad (50)$$

$$\text{SNR}_2 = \frac{|\rho| \sigma_Y^2}{\sigma_W^2 + (1 - |\rho|) \sigma_Y^2} = \frac{|\rho|}{\frac{\sigma_W^2}{\sigma_Y^2} + (1 - |\rho|)}. \quad (51)$$

Some observations about (50) and (51) follow.

1. SNR_1 and SNR_2 increase monotonically as $|\rho|$ increases.
2. SNR_1 (SNR_2) increases monotonically as σ_X^2 (σ_Y^2) increases, and for fixed $|\rho|$ is bounded by

$$\lim_{\sigma_X^2 \rightarrow \infty} \text{SNR}_1 = \lim_{\sigma_Y^2 \rightarrow \infty} \text{SNR}_2 = \frac{|\rho|}{1 - |\rho|}. \quad (52)$$

Thus a loud source (large σ_X^2, σ_Y^2) has larger coherent SNR, i.e., increasing σ_X^2, σ_Y^2 cannot reduce the coherent SNR, but the limit (52) cannot be exceeded for a given $|\rho|$.

3. If a particular coherent SNR is desired, then (52) implies a threshold coherence magnitude $|\rho|$ that is required to achieve that SNR, given by

$$|\rho| \geq \frac{\text{SNR}}{1 + \text{SNR}}. \quad (53)$$

Note that for large coherent SNR, nearly perfect coherence $|\rho| \approx 1$ is required.

The analysis extends to complex Gaussian random processes as follows. Consider a time delay estimation problem with two sensors and noisy observations of the form in (8),

$$z_1(t) = s_1(t) + w_1(t) \quad (54)$$

$$z_2(t) = s_2(t - D) + w_2(t), \quad (55)$$

where $w_1(t), w_2(t)$ are additive, white, Gaussian noise (AWGN) processes, $s_1(t), s_2(t)$ are partially coherent Gaussian random processes, and D is the time delay. The AWGN processes $w_1(t), w_2(t)$ have properties as in (9) with power spectral density (PSD) $G_w(\omega)$, and the signals $s_1(t), s_2(t)$ are characterized by the cross-spectral density matrix

$$\begin{bmatrix} s_1(t) \\ s_2(t) \end{bmatrix} \sim \begin{bmatrix} G_{s,11}(\omega) & \gamma_{s,12}(\omega) (G_{s,11}(\omega)G_{s,22}(\omega))^{1/2} \\ \gamma_{s,12}(\omega)^* (G_{s,11}(\omega)G_{s,22}(\omega))^{1/2} & G_{s,22}(\omega) \end{bmatrix}. \quad (56)$$

Then analogous to (43, (44)), $s_1(t)$ and $s_2(t)$ can be represented as

$$s_1(t) = h_1(t) * s(t) + n_1(t) \quad (57)$$

$$s_2(t) = h_2(t) * s(t) + n_2(t) \quad (58)$$

where $s(t), n_1(t), n_2(t)$ are independent, zero mean, circular, complex Gaussian random processes, $*$ denotes convolution, and

$$H_1(\omega) = G_{s,11}(\omega)^{1/2} \quad (59)$$

$$H_2(\omega) = \frac{\gamma_{s,12}(\omega)^*}{|\gamma_{s,12}(\omega)|} G_{s,22}(\omega)^{1/2} \quad (60)$$

$$G_s(\omega) = |\gamma_{s,12}(\omega)| \quad (61)$$

$$G_1(\omega) = G_{s,11}(\omega) [1 - |\gamma_{s,12}(\omega)|] \quad (62)$$

$$G_2(\omega) = G_{s,22}(\omega) [1 - |\gamma_{s,12}(\omega)|]. \quad (63)$$

$G_s(\omega)$, $G_1(\omega)$, $G_2(\omega)$ are the PSDs of $s(t)$, $n_1(t)$, $n_2(t)$, and $H_1(\omega)$, $H_2(\omega)$ are the frequency responses corresponding to $h_1(t)$, $h_2(t)$ that model the deterministic “channels” from source to sensors. Then (57),(58) can be inserted into (54),(55),

$$z_1(t) = (h_1 * s)(t) + n_1(t) + w_1(t) \quad (64)$$

$$z_2(t) = (h_2 * s)(t - D) + n_2(t) + w_2(t), \quad (65)$$

which fits the standard model for time delay estimation of *coherent* signals observed through linear filters in AWGN [20]. The partial signal coherence $\gamma_{s,12}(\omega)$ between $s_1(t)$, $s_2(t)$ in (54),(55) is equivalently modeled by the filtered coherent signals $(h_1 * s)$, $(h_2 * s)$ and the excess additive noise $n_1(t)$, $n_2(t)$.

References

- [1] R.J. Kozick and B.M. Sadler, “Distributed sensor array processing of wideband acoustic signals,” *IRIS Battlefield Acoustics Symposium*, September 1999.
- [2] T. Pham and B. M. Sadler, “Aeroacoustic wideband array processing for detection and tracking of ground vehicles,” *130th Meeting of the Acoustic Society of America*, St. Louis, MI, *JASA* vol. 98, no. 5, pt. 2, p. 2969, 1995.
- [3] T. Pham and B. M. Sadler, “Adaptive wideband aeroacoustic array processing,” *8th IEEE Statistical Signal and Array Processing Workshop*, pp. 295–298, Corfu, Greece, June 1996.
- [4] T. Pham and B. Sadler, “Incoherent and coherent wideband direction finding algorithms for ground vehicles,” *132nd Meeting of the Acoustic Society of America*, *JASA* vol. 100, no. 4, pt. 2, p. 2636, October 1996.
- [5] T. Pham and B. M. Sadler, “Focused wideband array processing algorithms for high-resolution direction finding,” *IRIS Battlefield Acoustics Symposium*, October 1998.
- [6] H. Wang and M. Kaveh, “Coherent signal-subspace processing for the detection and estimation of angles of arrival of multiple wide-band sources,” *IEEE Trans. Acoust., Speech, Signal Processing*, vol. ASSP-33, pp. 823–831, August 1985.
- [7] B. M. Sadler, “Focused wideband maximum likelihood and spatial spectrum estimation” *920th Meeting of the American Mathematical Society*, invited presentation for Special Session on Harmonic Analysis and Applications, College Park, MD, April 1997.
- [8] A. Paulraj and T. Kailath, “Direction of arrival estimation by eigenstructure methods with imperfect spatial coherence of wavefronts,” *J. Acoust. Soc. Am.*, vol. 83, pp. 1034–1040, March 1988.
- [9] A.B. Gershman, C.F. Mecklenbrauker, J.F. Bohme, “Matrix fitting approach to direction of arrival estimation with imperfect spatial coherence,” *IEEE Trans. on Signal Proc.*, vol. 45, no. 7, pp. 1894–1899, July 1997.
- [10] B.-G. Song and J.A. Ritcey, “Angle of arrival estimation of plane waves propagating in random media,” *J. Acoust. Soc. Am.*, vol. 99, no. 3, pp. 1370–1379, March 1996.
- [11] D.K. Wilson, “Performance bounds for acoustic direction-of-arrival arrays operating in atmospheric turbulence,” *J. Acoust. Soc. Am.*, vol. 103, no. 3, pp. 1306–1319, March 1998.

- [12] M. Wax and T. Kailath, "Decentralized processing in sensor arrays," *IEEE Trans. on Acoustics, Speech, Signal Processing*, vol. ASSP-33, no. 4, pp. 1123-1129, October 1985.
- [13] E. Weinstein, "Decentralization of the Gaussian maximum likelihood estimator and its applications to passive array processing," *IEEE Trans. Acoust., Speech, Sig. Proc.*, vol. ASSP-29, no. 5, pp. 945-951, October 1981.
- [14] A.J. Weiss and E. Weinstein, "Fundamental limitations in passive time delay estimation - part 1: narrowband systems," *IEEE Trans. Acoust., Speech, Sig. Proc.*, vol. ASSP-31, no. 2, pp. 472-485, April 1983.
- [15] D.K. Wilson, "Atmospheric effects on acoustic arrays: a broad perspective from models," *1999 Meeting of the IRIS Specialty Group on Battlefield Acoustics and Seismics*, Laurel, MD, September 13-15, 1999.
- [16] D.K. Wilson, G.L. Szeto, B.M. Sadler, R. Adams, N. Srour, "Propagation and array performance modeling for acoustic tracking of cruise missiles," *1999 Meeting of the IRIS Specialty Group on Battlefield Acoustics and Seismics*, Laurel, MD, September 13-15, 1999.
- [17] S.M. Kay, *Fundamentals of Statistical Signal Processing: Estimation Theory*, Prentice-Hall, 1993.
- [18] B. Friedlander, "On the Cramer-Rao Bound for Time Delay and Doppler Estimation," *IEEE Trans. on Info. Theory*, vol. IT-30, no. 3, pp. 575-580, May 1984.
- [19] P. Whittle, "The analysis of multiple stationary time series," *J. Royal Statist. Soc.*, vol. 15, pp. 125-139, 1953.
- [20] G.C. Carter (ed.), *Coherence and Time Delay Estimation* (Selected Reprint Volume), IEEE Press, 1993.
- [21] C.H. Knapp and G.C. Carter, "The generalized correlation method for estimation of time delay," *IEEE Trans. on Acoustics, Speech, Signal Processing*, vol. ASSP-24, no. 4, pp. 320-327, August 1976.